Investigation of self-sealing in high-strength and ultra-low-permeability concrete in water using micro-focus X-ray CT

Daisuke FUKUDA[1], Yoshitaka NARA[2], Yuya KOBAYASHI[3], Megumi MARUYAMA[1], Mayuko KOKETSU[1], Daisuke HAYASHI[4], Hideo OGAWA[5], Katsuhiko KANEKO[6]

[1] Graduate School of Engineering, Hokkaido University, Kita 13 Nishi 8, Kita-ku, Sapporo, Hokkaido 060-8628, Japan
[2] Graduate School of Engineering, Kyoto University, Kyoto 611-8540, Japan
[3] Graduate School of Engineering, Hokkaido University, Kita 13 Nishi 8, Kita-ku, Sapporo, Hokkaido 060-8628, Japan (Present address: Tokyo Gas Co. Ltd., 5-16-20 Kita Urawa, Urawa-ku, Saitama 330-0074, Japan)
[4] Taiheiyo Consultant Co., Ltd., Ohsaku, Sakura 285-8655, Japan (Present address: Radioactive Waste Management Funding and Research Center, Tsukishima 1-15-7, Chuo-ku, Tokyo, 104-0052, Japan)
[5] Taiheiyo Consultant Co., Ltd., Ohsaku, Sakura 285-8655, Japan
[6] Faculty of Engineering, Hokkaido University, Kita 13 Nishi 8, Kita-ku, Sapporo, Hokkaido 060-8628, Japan

*Corresponding author: Yoshitaka NARA
E-mail: nara.yoshitaka.2n@kyoto-u.ac.jp
TEL&FAX: +81-75-383-3211

Key words: crack, self-sealing, micro-focus X-ray CT, image subtraction, high-strength and ultra-low-permeability concrete

Abstract

High-strength and ultra-low-permeability concrete (HSULPC) is thought to be useful as a radioactive waste package. Thus, a high confining ability is desirable. For cementitious materials, sealing of cracks may occur in water due to the precipitation of calcium compounds. This can affect the confining ability. In this study, the sealing of a crack in HSULPC in water was investigated using micro-focus X-ray computed tomography (CT). The sealing by precipitation occurred only around the end of the specimen. Sealed regions of the crack were identified using three-dimensional image registration and CT image subtraction of images obtained for the specimen before and after it was immersed in water to evaluate temporal changes of the sealing deposits in the crack. The sealing deposits increased as the HSULPC specimen was kept in water longer. It was concluded that cracks in HSULPC in water are sealed by precipitation.

1. Introduction

For the geological disposal of radioactive wastes, the radioactivity intensity of the radionuclides can be reduced by engineered barriers, such as bentonite buffers, and natural barriers, such as rock mass. If a repository of radioactive waste is located in an area where the hydraulic gradient and the permeability are high, the retardation of radionuclide migration by these barriers may not be sufficient. To retard the migration, several alternative concepts of radioactive waste packages are being developed. High-strength and ultra-low-permeability concrete (HSULPC) is planned for radioactive waste packages for the geological disposal of transuranic (TRU) waste [1–3] to confine the radionuclides with low adsorption by the engineered barriers, such as C-14 included in TRU waste in Japan.

Generally, water migrates through networks of cracks and pores in a solid. In cementitious materials, precipitation, mainly of calcium compounds, occurs in water. Thus, the sealing of cracks and pores by precipitation can occur, and this may affect permeability. This phenomenon has been investigated by various researchers [4–12]. Edvardsen [7] showed that sealing of a crack occurs by precipitation of calcium carbonate, generated from CO_3^{2-} in water and Ca^{2+} in cement paste. The crack width and applied water pressure affected the sealing significantly, but the composition of the surrounding water had little effect [7]. Yang et al. [11] showed that sealing occurs if the crack width is less than 0.15 mm. Reinhardt and Jooss [8] investigated the temperature dependence of the sealing and showed that sealing is enhanced with increasing temperature, up to 80°C.

Because a high confining ability is required for HSULPC, detailed investigation of the sealing of cracks and pores in water is of considerable importance. It is thus important to observe the sealing of cracks and pores directly. X-ray computed tomography (CT) scanners are an effective tool for observing the sealing of cracks and pores, because we can observe not only the surface but also the interior of the material with this non-destructive technique. Specifically, we can observe the details of the sealing of cracks and pores in HSULPC using micro-focus X-ray CT, because images with high resolution can be obtained. However, to date, observations of this sort have not been reported. Additionally, the temporal behavior of sealing has not yet been clarified.

In this study, we investigated the sealing of cracks in HSULPC in water using micro-focus X-ray CT.

2. Sample

HSULPC made by Taiheiyo Co., Ltd., was used. Because detailed information about the material properties of HSULPC has been reported previously by Nara et al. [13], we provide only the composition of the HSULPC in Table 1.

Fig. 1 shows a photograph of the cracked HSULPC specimen used in this study. An initially intact cylindrical specimen of HSULPC was split in half axially using the Brazil test technique, and was set in an acrylic cylinder tube. The initial crack width was approximately 0.1 mm throughout the specimen. The height of the acrylic cylinder tube was 35 mm. The diameter and height of the HSULPC specimen were approximately 13 mm and 15 mm, respectively.

3. Observation by X-ray CT

3.1. Observation method

In Japan, salt water is often found underground [14–16]. Thus, considering the condition of groundwater in Japan, the HSULPC specimen was kept in simulated seawater inside a plastic bottle. Table 2 shows the chemical composition of the simulated seawater used. When the specimen was kept in water, a vacuum desiccator was used to ensure that water would fill the entire crack. The amount (weight) of water used was ten times larger than the weight of the HSULPC specimen. To avoid the undesirable dissolution of CO_2 in the water, the air in the plastic bottles was replaced with nitrogen gas. The specimen was kept in a thermostatic chamber at a temperature of 293 K. Because X-rays are more or less attenuated by the presence of water and this causes undesirable error in the image analysis, as discussed below, the HSULPC specimen was dried for a day at room temperature before each X-ray CT observation so as to remove the water from the specimen. The observations were conducted at the start and after keeping the specimen in water for 1, 3, and 7 weeks.

For the observation by X-ray CT, a micro-focus X-ray CT scanner, TOSCANER 31300μhd (Toshiba IT & Control Systems Co., Ltd.), installed at Hokkaido University, Japan, was used. The applied tube voltage and maximum tube current were 130 kV and 62 μA, respectively, which were used in each scan in this study. For X-ray CT scanning, cone-beam scanning mode [17] was used in which multiple CT images, up to several hundred cross sections, were provided through one scan, and quick three-dimensional (3D) reconstruction of specimen was possible. The number of pixels in each cross section was 1024 × 1024 corresponding to 16 μm × 16 μm for each pixel. The notion of a "voxel" is used in X-ray CT, defined as a pixel having some thickness, named the slice thickness. Here, the slice thickness was 24 μm.

During scanning, the observed specimen is placed on a table and the table rotates continuously with the relative positions between the X-ray tube and detector, named an X-ray image intensifier, being fixed. The number of projection directions used in all scans was 1500 (i.e., the interval between each projection angle was 2π/1500 radians). In each projection direction, 20 consecutive scans were conducted and averaged projection data were used for image reconstruction to reduce statistical noise caused in the X-ray image intensifier. The linear attenuation coefficient [18], μ, for each voxel was computed from the projection data with an image reconstruction algorithm, based on a filtered back-projection method [17, 19] in which a Ramachandran-Lakshminarayanan filter function [20] was used. Then, CT images were reconstructed through the CT values, calculated as follows:

$$V_{\mathrm{ct}} = S\mu + B \tag{1}$$

where V_{ct} is the CT value, which is a signed integer taking a value between −8192 and 8191, and S and B are both constants. In this study, S and B were 200 and 0, respectively. The CT values in Eq. (1) are not defined in Hounsfield units, as found in many industrial X-ray CT scanners. For noise reduction measures, which are quite important in X-ray CT, a reduction in undesirable effects of scattered X-rays on the X-ray image intensifier was achieved using an X-ray collimator set in front of X-ray tube. Additionally, two notorious artifacts, the cupping effect, due to beam hardening, and the ring artifact [17, 18], were minimized using a copper filter with a thickness of 0.1 mm in a so-called “gain calibration” [18].

Based on the considerations above, 680 CT slice images in total were obtained to reconstruct the entire crack in the HSULPC specimen by X-ray CT scanning and to identify the precipitated regions.

3.2. Results

A typical CT slice image at one cross section of the specimen before it was kept in seawater is shown in Fig. 2. The cross section also corresponds to the top in the image analysis described in Section 4. Based on a window level of 400 and a window width of 1200, this image is presented in gray-scale with a range of 256 shades from black to white. High CT values, shown in white or brighter colors, correspond to regions with higher density. Regions of low CT values, shown in black or darker colors, correspond to areas of lower density. The black zigzag line found in the central part of the image is the crack, and the dark circular shapes of various sizes are pores. Small white granular regions having higher density are also found over the whole slice and these correspond to metal included in the silica fume as a byproduct of metal refining. The other regions, shown in gray colors, are the matrix of HSULPC, consisting of cement and aggregates.

It was observed from the CT images that most of the pores with their diameters approximately greater than ten micrometers were isolated from each other, although some of the pores were on the surface of the specimen. Additionally, some pores were connected to the crack. It may be possible that pores of much smaller sizes (< 1 μm) are connected, which are not observable at the resolution of the used CT scanner. Fig. 3 shows CT images of the crack, for approximately the same cross section, extracted from seven CT images of a specimen before it was immersed in seawater and after it was kept in seawater for 7 weeks. These images are presented at intervals of 48 μm from one end to the interior of the specimen. In the region close to the end, most parts of the crack were sealed in the HSULPC specimen kept in seawater for 7 weeks. In contrast, less sealing was observed towards the interior of the specimen. Although most parts were sealed in the crack closer to the end, the CT image of the corresponding part showed blurring due to the so-called “partial volume effect” [18], where voxels are affected by including both precipitates and air within them. Blurring is also caused by the tilted surface of the specimen at the ends. From these results, sealing of the crack by precipitation generally occurred only near the end of the specimen.

Fig. 4 shows the temporal change in sealing of the crack for one cross section. These cross sections are the same sections as Fig. 2 and those indicated by dotted lines in Fig. 3(a). The occurrence of precipitation was observed after the specimen was kept in water for 1 week. Additionally, the sealed area increased with elapsed time. Because no re-opening of the sealed crack was found, dissolution of the precipitates did not occur over the period of observation. No swelling of the specimen was found during the period of observation.

The following observations were clarified by the X-ray CT. The occurrence of significant precipitation was found from the end to the interior of the specimen within a range of approximately 0.2 mm, and the total amount of precipitate increased with elapsed time in the region closer to the end. Most parts of the crack were sealed after 7 weeks due to precipitation near the end. Once such sealing was achieved, no further precipitation was observed in the crack below the sealed part.

A photograph of the end of the specimen kept in seawater is shown in Fig. 5. Precipitation occurred in such a way that the precipitates covered over the end.

Based on these results, image analyses were conducted to evaluate the sealing process only near the end of the specimen, where significant precipitation was observed in the crack.

4. Image analysis

4.1 Image processing method

To investigate temporal changes in the sealed regions of the crack, it was necessary to extract the sealed regions by image processing. For the cross sections where sealing was observed, we sought to extract precipitates by applying an image subtraction technique between the CT images before and after the specimen was kept in water. However, due to the need to set the specimen on the table in the CT scanner manually before each scan, an alignment gap between the comparison images occurred. Thus, before conducting the image subtraction, image registration was used to minimize the alignment gap. For this purpose, an affine linear transformation, expressed by the following equation, was used:

$$u_i = \alpha_{i1} + \alpha_{i2} \cdot x + \alpha_{i3} \cdot y + \alpha_{i4} \cdot z \quad (i = 1, 2, 3) \qquad (2)$$

where u_i indicates the alignment gap of corresponding voxels between comparison images in three directions, defined in Cartesian coordinates, and (x, y, z) indicate the integer coordinates of each voxel in the reference CT images. CT images before the specimen was kept in water were used as the reference images, and CT images after the specimen was kept in water were mapped onto the reference integer coordinates. In each direction, four unknown coefficients, α_{ij}, need to be determined.

Here, we explain how to determine α_{ij}. In Fig. 6, a 3D image of the upper half of a HSULPC specimen kept in seawater is shown. Distinctly white granular regions are included in the image. We used these granular regions to determine α_{ij}. The region of interest (ROI) was set as a rectangular parallelepiped. The thickness corresponding to 30 slices from the end to the interior of the specimen was included. The matrix size of the ROI was 342 × 342 in the center of each slice. In the ROI of reference images, 11 sampling points were selected where the white granular regions took their local maximum values. Then, approximate values of u_i in Eq. (2) for the 11 points were obtained by a least squares method. Then, to obtain more precise values of α_{ij}, the volumetric cross-correlation, C, defined in the following equation was introduced:

$$C = \iiint_{\mathrm{ROI}} f_0(x, y, z) \cdot f_{\mathrm{R}}(x + u_1, y + u_2, z + u_3)\, dxdydz \qquad (3)$$

where f_0 is the spatial distribution of CT values in the reference images and f_R is that of comparison images, transformed by u_i of the given α_{ij}. We considered that α_{ij} became optimal when C took the maximum value in the ROI. Because the nearest cross section to the end resulted in blurred CT images (see Fig. 3) and they might cause significant error in the image analysis, blurred CT images were excluded from the top of the ROI. Consequently, the top cross sections of the ROI were those surrounded by dashed lines in Fig. 3(a).

4.2 Results

The results of the image subtraction (i.e., subtraction images) are shown in Fig. 7. The reference images correspond to those obtained for the initial specimen before immersion in seawater. Comparison images were obtained after 1, 3, or 7 weeks in seawater. In the figure, only the cracks in the ROI are presented at an interval of 48 μm from the top to the interior of the ROI. These images are displayed in gray-scale, with a range of 256 shades from black to white, for a window level and width of 0 and 1000, respectively. In regions where no change occurred, the difference between the CT values was approximately zero, displayed as a gray color in the subtraction images. In regions where precipitation occurred, the difference between the CT values was positive, displayed as a white color. Fig. 7 shows that the region of precipitation observed in Fig. 3 was successfully extracted from the crack.

In the subtraction images, reasonable segmentation between precipitated and non-precipitated regions was required. If a voxel includes both phases (i.e., precipitated and non-precipitated regions), the CT value, and, accordingly, differences in CT values, of this voxel takes an intermediate CT value between these two phases. Such a voxel is called a “mixel” [21-24]. Based on this, a maximum likelihood thresholding method considering the effect of mixels [21–23] was used to set an appropriate threshold, t. The threshold was determined from the histogram obtained in the boxed area A_t in Fig. 8(a). Fig. 8(a) shows the same cross section surrounded by dashed lines in Fig. 7(c). The histogram of the probability density function is shown in Fig. 8(b). The threshold determined from the maximum likelihood thresholding method was t = 182. Binarized images obtained from the subtraction images in Fig. 7 using this threshold are shown in

Fig. 9. The images show the cross sections from the top to the interior of the ROI at an interval of 48 μm, and demonstrate that the geometry of the precipitate was successfully segmented using the threshold.

5. Discussion

The X-ray CT observation results in Section 3 showed that sealing of the crack by precipitation occurred only near the end of the crack in the specimen. In this region, most parts were sealed. This suggests that the crack near the ends was in an environment where precipitation of calcium compounds, such as calcium carbonate, was enhanced by the calcium ions dissolved from the HSULPC and both the carbonate and bicarbonate ions found in the seawater.

If the crack is completely sealed near the end, the network of cracks inside the HSULPC can be isolated from the surrounding environment, which can cause a decrease in permeability [25] and retard degradation in terms of the confining ability of the HSULPC. Because the CT observations suggest that the sealed regions spread with elapsed time, an investigation of the temporal change of the sealing deposits could provide important information to evaluate the effect of the precipitates on limiting water flow into HSUPLC. Thus, we investigated the temporal change of the sealing deposits in the crack.

The 30 binarized images obtained in the previous section were used to evaluate the sealing. Fig. 10 shows a schematic illustration of precipitation in the crack. The percentage of sealing deposits in the crack, P_{seal}, in each slice, having slice thickness T_{slice}, was calculated. P_{seal} was calculated as follows:

$$P_{\mathrm{seal}} = \frac{T_{\mathrm{slice}} S_{\mathrm{pre}}}{T_{\mathrm{slice}} S_{\mathrm{crack}}} \times 100 = \frac{l^2 N_{\mathrm{pre}}}{l^2 N_{\mathrm{crack}}} \times 100 = \frac{N_{\mathrm{pre}}}{N_{\mathrm{crack}}} \times 100 (\%) \quad (4)$$

where T_{slice} is the slice thickness, S_{pre} is the total area of precipitates, S_{crack} is the total area of the crack, l is the pixel size (16 μm), and N_{pre} and N_{crack} are the numbers of pixels for precipitates and the crack, respectively, in ROI_1 in Fig. 9. N_{pre} in ROI_1 was obtained from the extracted precipitates in the binarized images. N_{crack} was obtained by counting the number of pixels corresponding to the crack in ROI_1 by applying the maximum likelihood thresholding method to the reference CT images before the specimen was kept in water, where the regions of the crack and matrix of the HSULPC were segmented. Because the mean value of the crack width in ROI_1 was approximately constant, the temporal change in P_{seal}, denoted as V_{seal}, was computed using the following equation:

$$V_{\mathrm{seal}} = \frac{\Delta P_{\mathrm{seal}}}{\Delta t} \left(\% \cdot \mathrm{day}^{-1}\right) \quad (5)$$

where ΔP_{seal} is the change in P_{seal} over the given immersion period, Δt.

P_{seal} in ROI_1 is shown in Fig. 11 with respect to the depth from the top to the interior of ROI_1. From this figure, P_{seal} became larger towards the end in each period, and P_{seal} within a depth of 0.05 mm also increased with elapsed time.

Similarly, V_{seal} in ROI_1 is shown in Fig. 12 with respect to the depth from the top to the interior of ROI_1. From this figure, V_{seal} towards the end became larger than in the inner region. The maximum V_{seal} was found at 3 weeks, after which V_{seal} started to decrease. This suggests that little sealing could be expected to occur after 7 weeks in ROI_1.

Based on the investigations described above, when HSULPC is kept in water, precipitation, such as of calcium compounds, occurs in the crack near the end, and the sealed regions or sealing deposits increase with elapsed time. Considering the application of HSULPC, it is desirable that such sealing should occur over a short period time. Thus, identifying optimum water conditions and crack widths is of considerable importance. To achieve this, more detailed investigation regarding the influence of water conditions on sealing and the change in water content due to precipitation could also be important. Additionally, considering that the temperature in the surrounding environment changes and that heat release occurs due to the exothermic reactions of radioactive waste, the temperature-dependency of the sealing behavior also needs to be further investigated. However, these investigations are beyond the scope of the present study, and we regard them as future work. The results reported in this paper could be important for engineering projects such as the geological disposal of radioactive wastes, and further accumulation of relevant information is important.

5. Conclusions

Sealing of crack in HSULPC was investigated in this study. A cracked HSULPC specimen was prepared and kept in simulated seawater for up to 7 weeks. The surface and interior of the cracked HSULPC specimen were then observed using micro-focus X-ray CT.

The results revealed that sealing of the crack occurred only near the end of the specimen. The occurrence of significant precipitation was found within approximately 0.05 mm from the end.

Temporal changes in sealing in the crack showed that the sealing deposits increased with the time the specimen was kept in water. Additionally, the sealing deposits increased towards the end of the HSULPC specimen.

Acknowledgements

DF was supported by research fellowships from the Japan Society for the Promotion of Science for Young Scientists. We also appreciate the help and advice from the Radioactive Waste Management Funding and Research Center.

References

[1] T. Kawasaki, H. Asano, H. Owada, A. Otsuki, T. Yoshida, T. Matsuo, K. Shibuya, A. Takei, Development of waste package for TRU-disposal(4) – Evaluation of confinement performance of TRU waste package made of high-strength and ultra low-permeability concrete-, Proceedings of GLOBAL 2005, Tsukuba, Japan, Oct. 2005, Paper No. 254.

[2] H. Owada, A. Otsuki, H. Asano, Development of waste package for TRU-disposal(1) – Concepts and performances, Proceedings of GLOBAL 2005, Tsukuba, Japan, Oct. 2005, Paper No. 351.

[3] K. Shibuya, H. Asano, H. Owada, A. Otsuki, T. Kawasaki, T. Yoshida, T. Matsuo, A. Takei, Development of waste package for TRU-disposal(3) - Examination of manufacturing technique of TRU waste package made of high-strength and ultra low-permeability concrete-, Proceedings of GLOBAL 2005, Tsukuba, Japan, Oct. 2005, Paper No. 256.

[4] S. Jacobsen, E.J. Sellevold, Self healing of high strength concrete after deterioration by freeze/thaw, Cem. Concr. Res. 26 (1996) 55–62.

[5] N. Hearn, C.T. Morley, Self-sealing property of concrete – Experimental evidence, Mater. Struct. 30 (1997) 404–411.

[6] N. Hearn, Self-sealing, autogenous healing and continued hydration: What is the difference?, Mater. Struct. 31 (1997) 563–567.

[7] C. Edvardsen, Water permeability and autogenous healing of cracks in concrete, ACI Mater. J. 96 (1999) 448–455.

[8] H. Reinhardt, M. Jooss, Permeability and self-healing of cracked concrete as a function of temperature and crack width, Cem. Concr. Res. 33 (2003) 981–985.

[9] S. Granger, A. Loukili, G. Pijaudier-Cabot, G. Chanvillard, Experimental characterization of the self-healing of cracks in an ultra high performance cementitious material: Mechanical tests and acoustic emission analysis, Cem. Concr. Res. 37 (2007) 519–527.

[10] S. Qian, J. Zhou, M.R. de Rooij, E. Schlangen, G. Ye, K. van Breugel, Self-healing behavior of strain hardening cementitious composites incorporating local waste materials, Cem. Concr. Compos. 31 (2009) 613–621.

[11] Y. Yang, M.D. Lepech, E.H. Yang, V.C. Li, Autogenous healing of engineered cementitious composites under wet-dry cycles, Cem. Concr. Res. 39 (2009) 382–390.

[12] T.H. Ahn, T. Kishi, Crack Self-healing behavior of cementitious composites incorporating various mineral admixtures, J. Adv. Concr. Technol. 8 (2010) 171–186.

[13] Y. Nara, M. Takada, D. Mori, H. Owada, T. Yoneda, K. Kaneko, Subcritical crack growth and long-term strength in rock and cementitious material, Int. J. Fract. 164 (2010) 57–71.

[14] M. Mizukami, H. Sakai, O. Matsubaya, Na-Ca-Cl-SO_4-type submarine formation waters at the Seikan undersea tunnel, Japan. Chemical and isotopic documentation and its interpretation, Geochim. Cosmochim. Acta 41 (1977) 1201–1212.

[15] T. Iwatsuki, R. Furue, H. Mie, S. Ioka, T. Mizuno, Hydrochemical baseline condition of groundwater at the Mizunami underground research laboratory (MIU), Appl. Geochem. 20 (2005) 2283–2302.

[16] K. Hama, T. Kunimaru, R. Metcalfe, A.J. Martin, The hydrogeochemistry of argillaceous rock formations at the Horonobe URL site, Japan, Phys. Chem Earth 32 (2007) 170–180.

[17] T.M. Buzug, *Computed Tomography: From Photon Statistics to Modern Cone-Beam CT*, first ed., Springer, New York, United States of America, 2008.

[18] R.A. Ketcham, W.D. Carlson, Acquisition, optimization, and interpretation of X-ray computed tomographic imagery: Applications to the geosciences, Comput. Geosci. 27 (2001) 381–400.

[19] A.C. Kak, M. Slaney, *Principles of Computerized Tomographic Imaging*, Society for Industrial and Applied Mathematics, Philadelphia, Pennsylvania, United States of America, 2001.

[20] G.N. Ramachandran, A.V. Lakshminarayanan, Three-dimensional reconstruction from radiographs and electron micrographs: Application of convolutions instead of Fourier transforms, Proc. Natl. Acad. Sci. U.S.A. 68 (1971) 2236–2240.

[21] A. Kitamoto, M. Takagi, Estimating the Area Proportions of Mixels Using Mixture Density Estimation with Mixel Densities: Trans. IEICE, J81-D-II (1998) 1160−1172 (in Japanese with English abstract).

[22] A. Kitamoto, A maximum likelihood thresholding methods considering the effect of mixels, Technical Report of IEICE (Institute of Electronics, Information, and Communication Engineers), Vol. PRMU99-166 (1999) 7−14 (in Japanese with English abstract).

[23] A. Kitamoto, M. Takagi, Image classification using probabilistic models that reflect the internal structure of mixels, Anal. Appl. 2 (1999) 31−43.

[24] H.S. Choi, D.R. Haynor, Y. Kim, Partial volume tissue classification of multichannel magnetic resonance images – A mixel model, IEEE Trans. Med. Imaging 10 (1991) 395–407.

[25] Y. Gueguen, J. Dienes, Transport properties of rocks from statistics and percolation, Math. Geol. 21 (1989) 1−13.

Figure legends

Fig. 1. Photograph of a cracked HSULPC specimen. The height and diameter of the HSULPC were 15 mm and 13 mm, respectively. The crack width was 0.1 mm. (a): General view, (b): top view.

Fig. 2. X-ray CT sliced image of a cracked HSULPC specimen before it was kept in seawater.

Fig. 3. Comparison of corresponding CT images of the crack: (a): before immersion in seawater, (b): after it was kept in seawater for 7 weeks. The height and width of each image are 11 mm and 1 mm, respectively.

Fig. 4. Comparison of CT images for a particular section. The height and width of each image are 11 mm and 1 mm, respectively.

Fig. 5. Photograph of precipitation that occurred over the end of the HSULPC specimen when it was kept in seawater. The regions with the white coloration correspond to precipitates.

Fig. 6. 3D CT image of the upper half of the HSULPC specimen used in the image analysis, where the ROI used in the image registration given by Eqs. (2) and (3) is indicated by the rectangular parallelepiped.

Fig. 7. Subtraction between the initial reference image and ones obtained after the specimen was kept in seawater for (a) 1, (b) 3, or (c) 7 weeks. The height and width of each subtraction image are 3.04 mm and 0.64 mm, respectively.

Fig. 8. Subtraction image and histogram for probability density of CT values used to determine a threshold. (a) Subtraction image. Region A_t was used to determine the threshold segmenting the precipitated and non-precipitated parts. (b) Histogram obtained from A_t, where the threshold was determined from the maximum likelihood thresholding method considering the effect of mixels.

Fig. 9. Binarized images obtained for the differences between reference images and images after the specimen was kept in seawater for (a) 1, (b) 3, and (c) 7 weeks. The height and width of each subtraction image are 3.04 mm and 0.64 mm, respectively. The crack width in ROI_1 was 0.06 mm.

Fig. 10. Schematic diagram of precipitation on the surface of the crack in each slice.

Fig. 11. Relationship between the percentage and position of the sealing deposits in specimen kept in seawater for 1, 3, and 7 weeks.

Fig. 12. Temporal change of the percentage of the sealing deposits for specimen kept in seawater for 1, 3, and 7 weeks.

Table legends

Table 1. Composition of HSULPC (after Nara et al. [13]).

Table 2. Chemical composition of simulated seawater (mol/L).

Tables

Table 1. Composition of HSULPC (after Nara et al. [13]).

	Amount [kg/m^3]
Low-heat Portland cement	744 – 1014
Silica fume	158 – 496
Fillers (fly ash, blast furnace slag, etc.)	225 – 541
Aggregates	631 – 947
Water-reducing admixture	24
Water	180

Table 2. Chemical composition of simulated seawater (mol/L).

Ca^{2+}	10×10^{-3}
SO_3^{2-}	29×10^{-3}
Na^{+}	45×10^{-2}
K^{+}	19×10^{-3}
Cl^{-}	56×10^{-2}
Mg^{2+}	55×10^{-3}
HCO_3^{-}	24×10^{-4}

Figure1

Click here to download high resolution image

(a) (b)

Figure2
Click here to download high resolution image

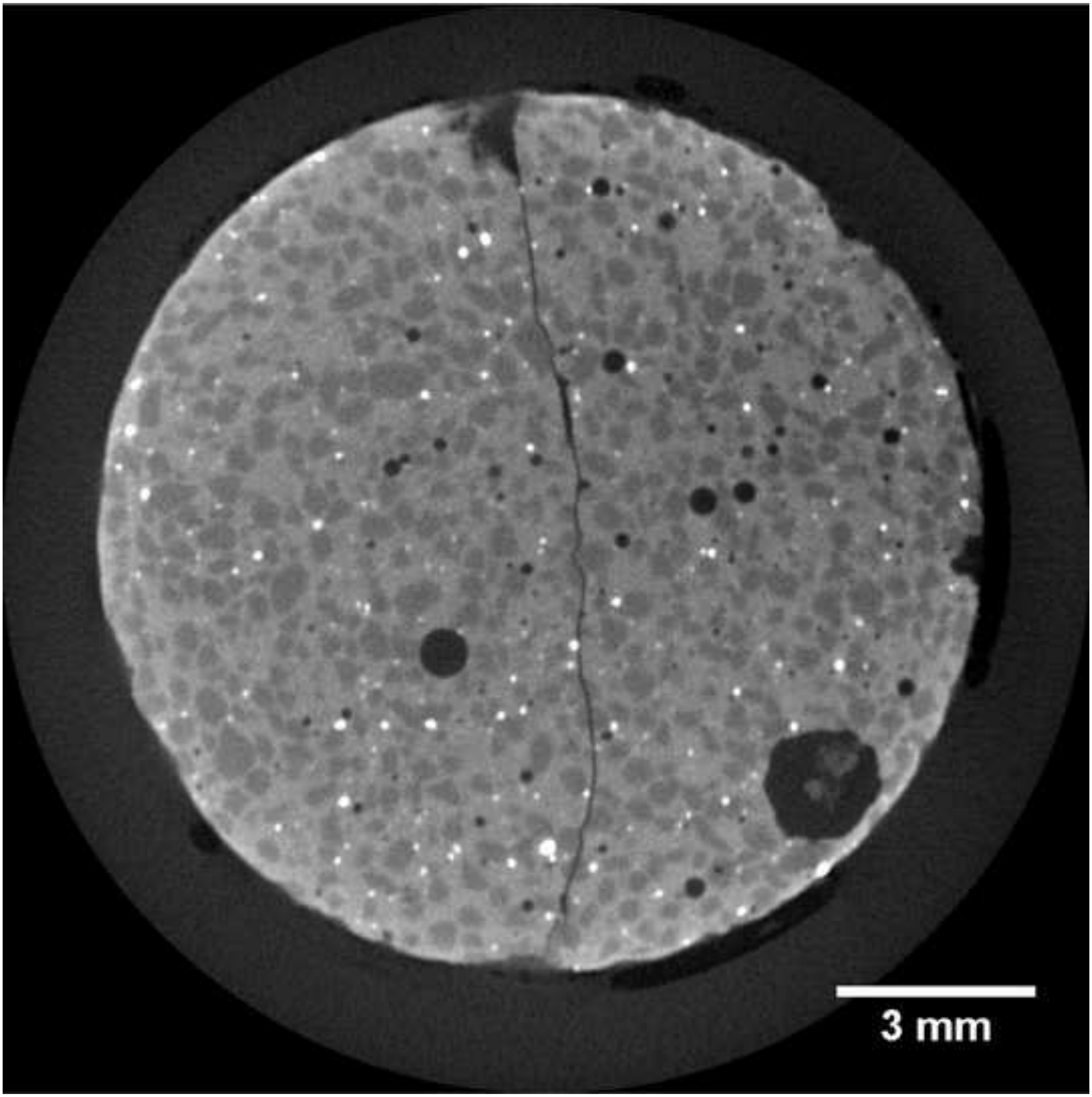

Figure3a
Click here to download high resolution image

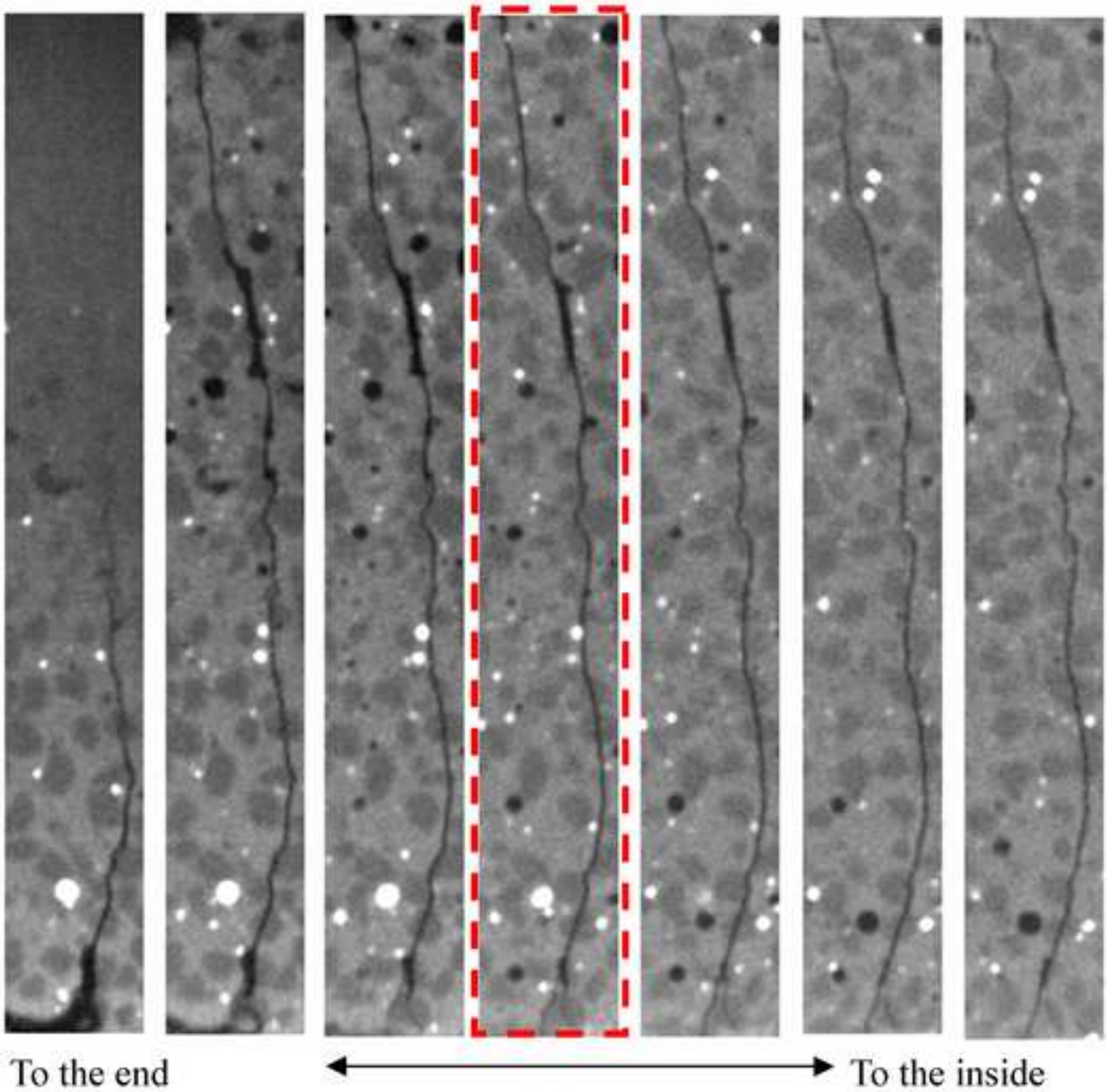

(a)

Figure3b
[Click here to download high resolution image]

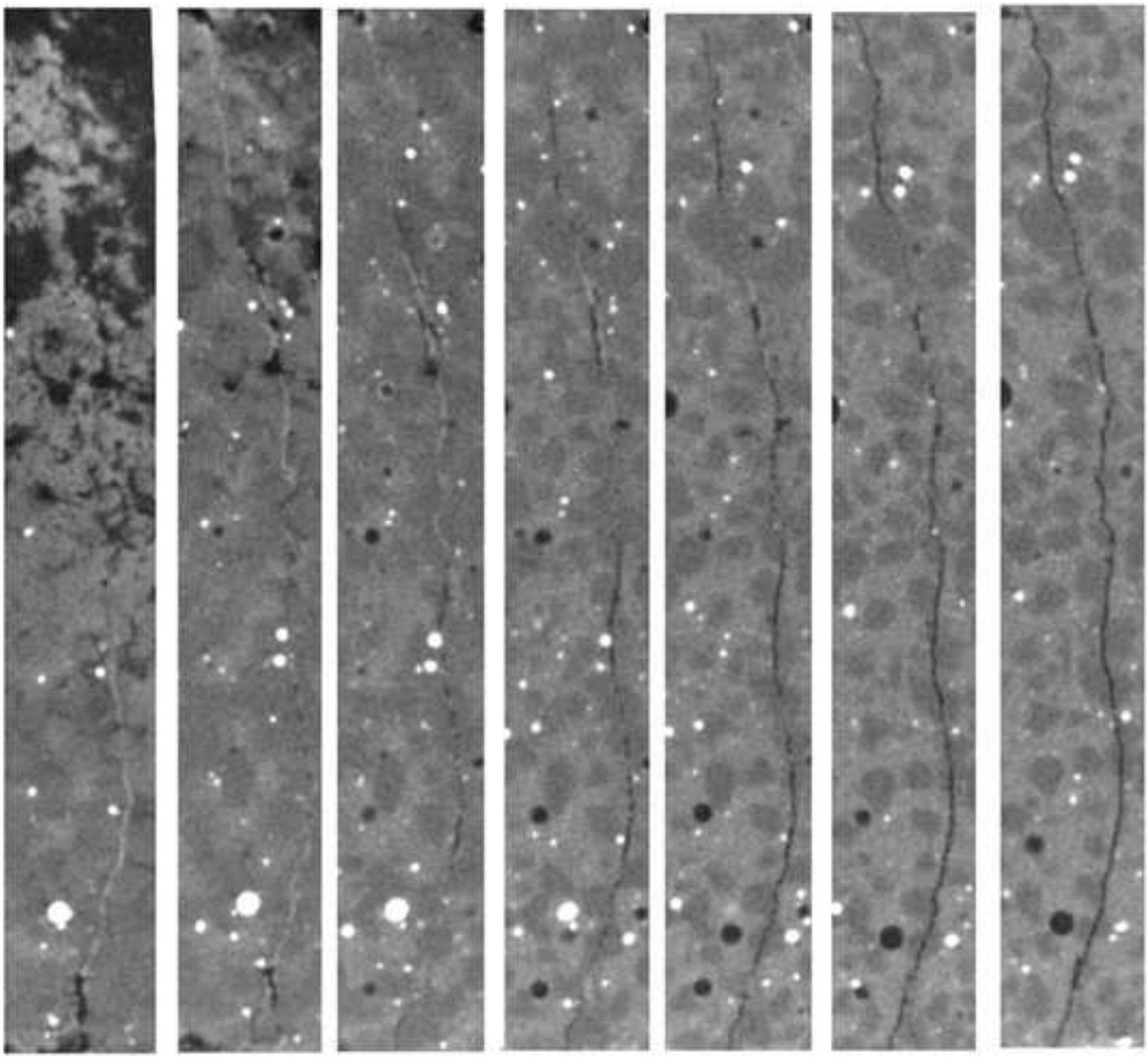

(b)

Figure4
Click here to download high resolution image

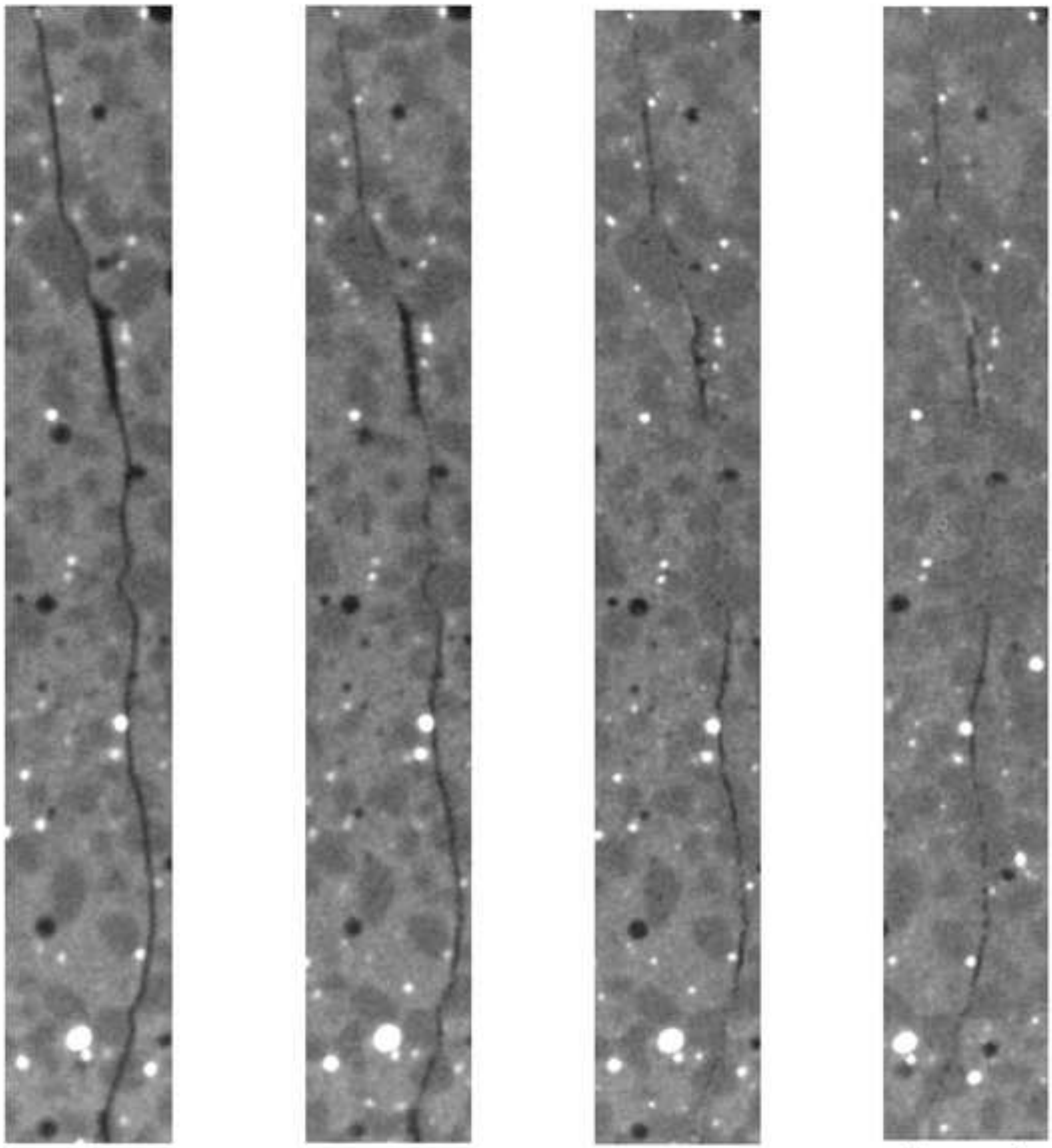

Figure5
Click here to download high resolution image

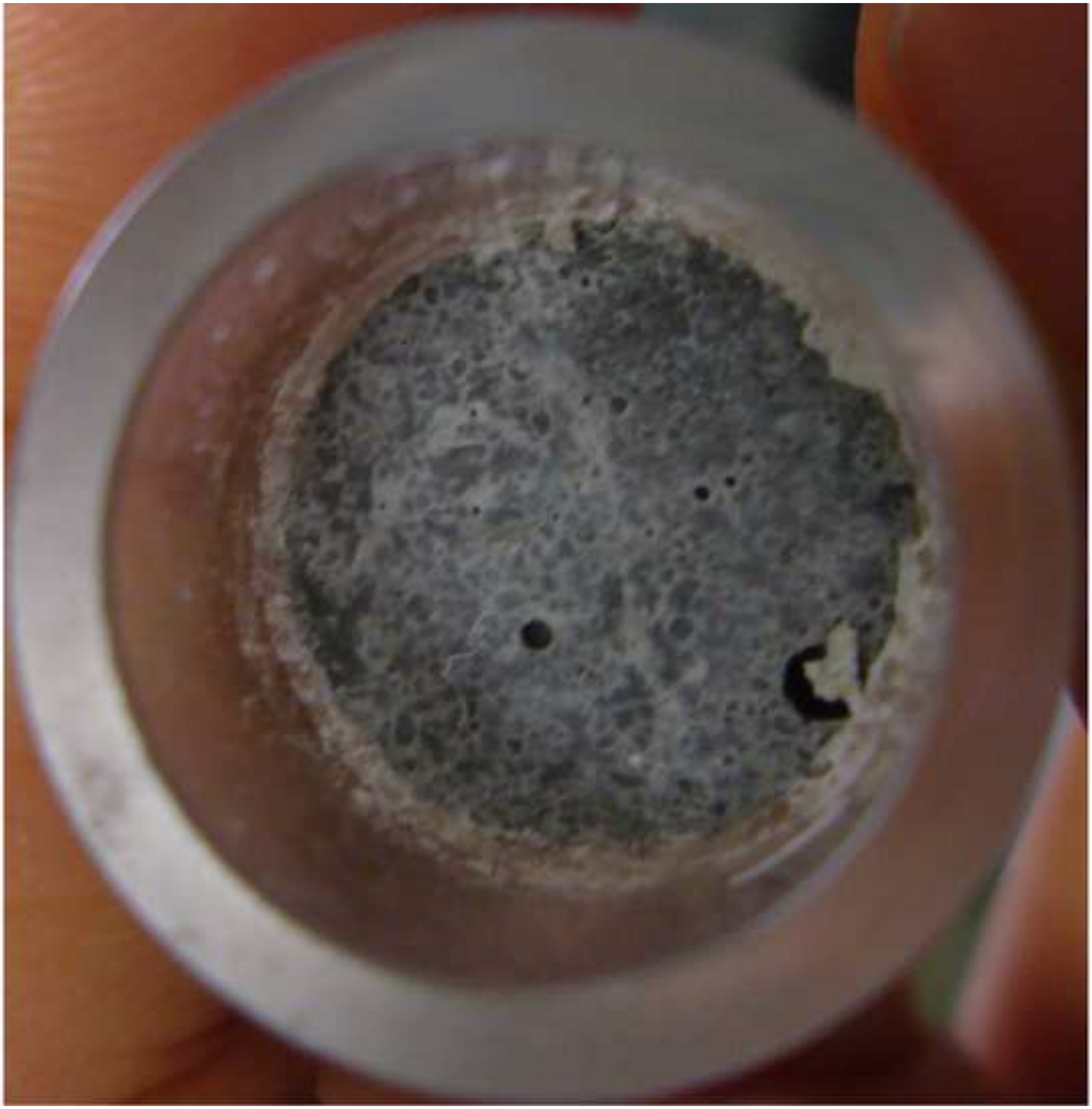

Figure6
Click here to download high resolution image

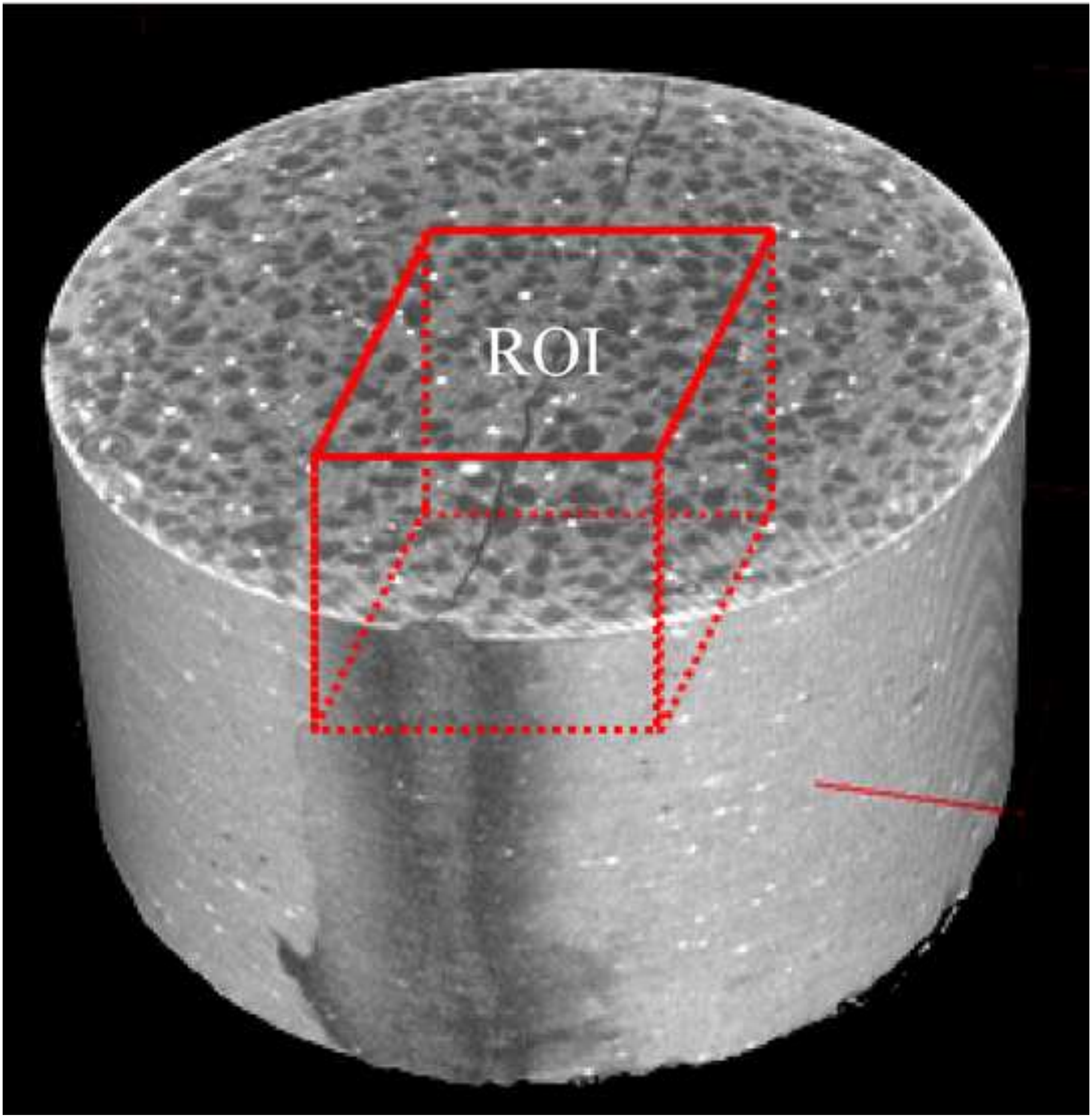

Figure7
Click here to download high resolution image

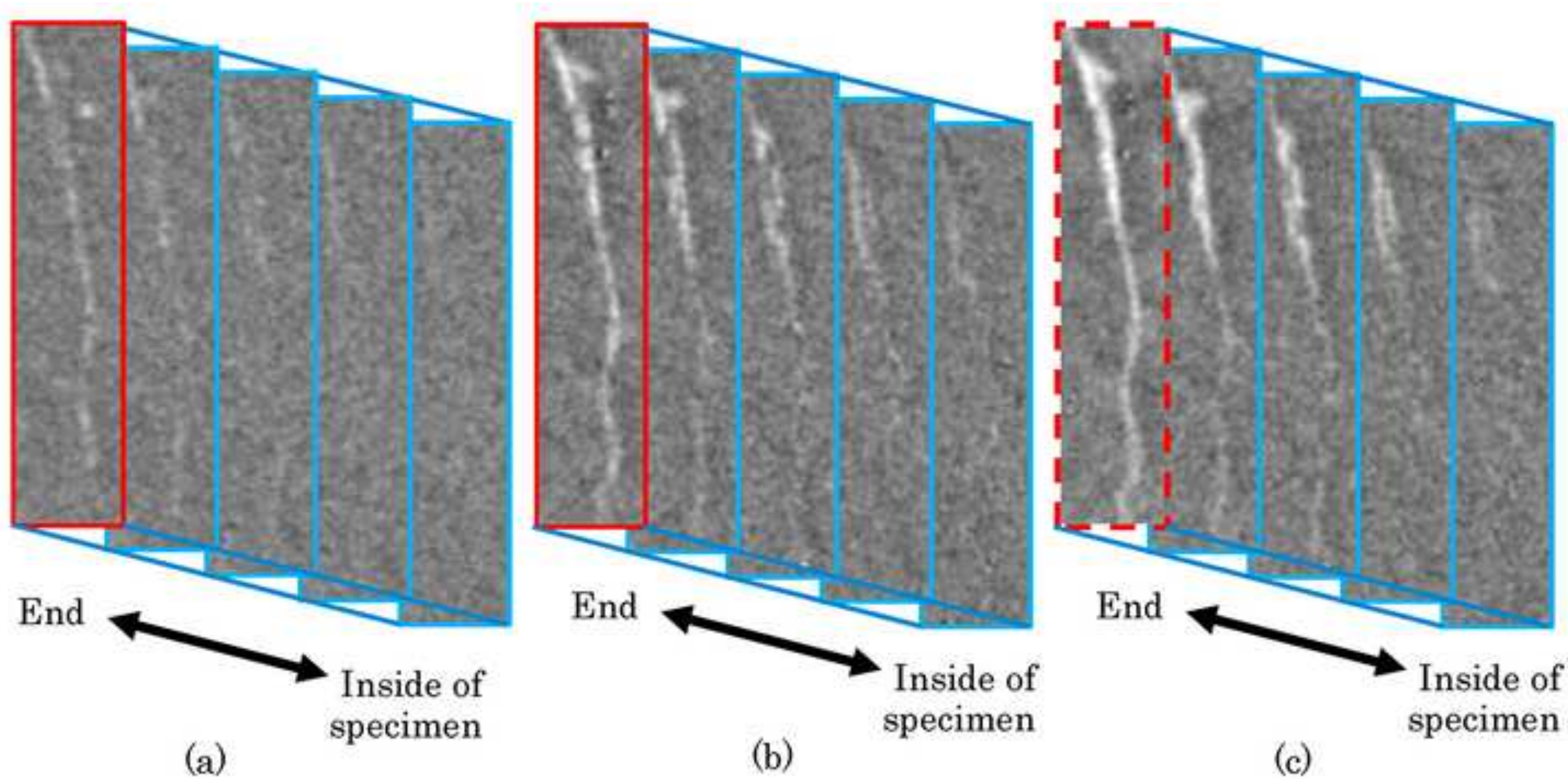

Figure8
Click here to download high resolution image

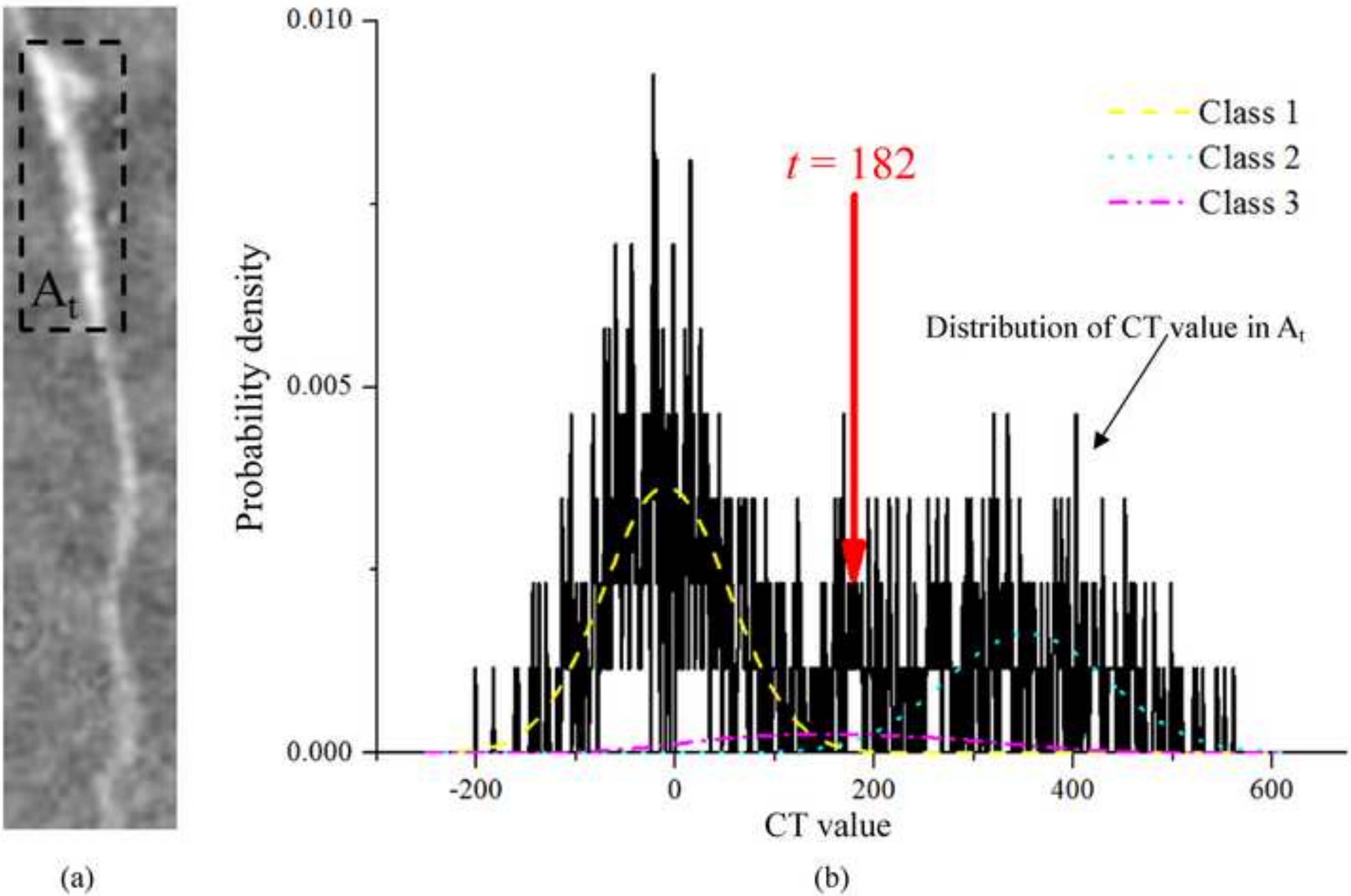

Figure9

Click here to download high resolution image

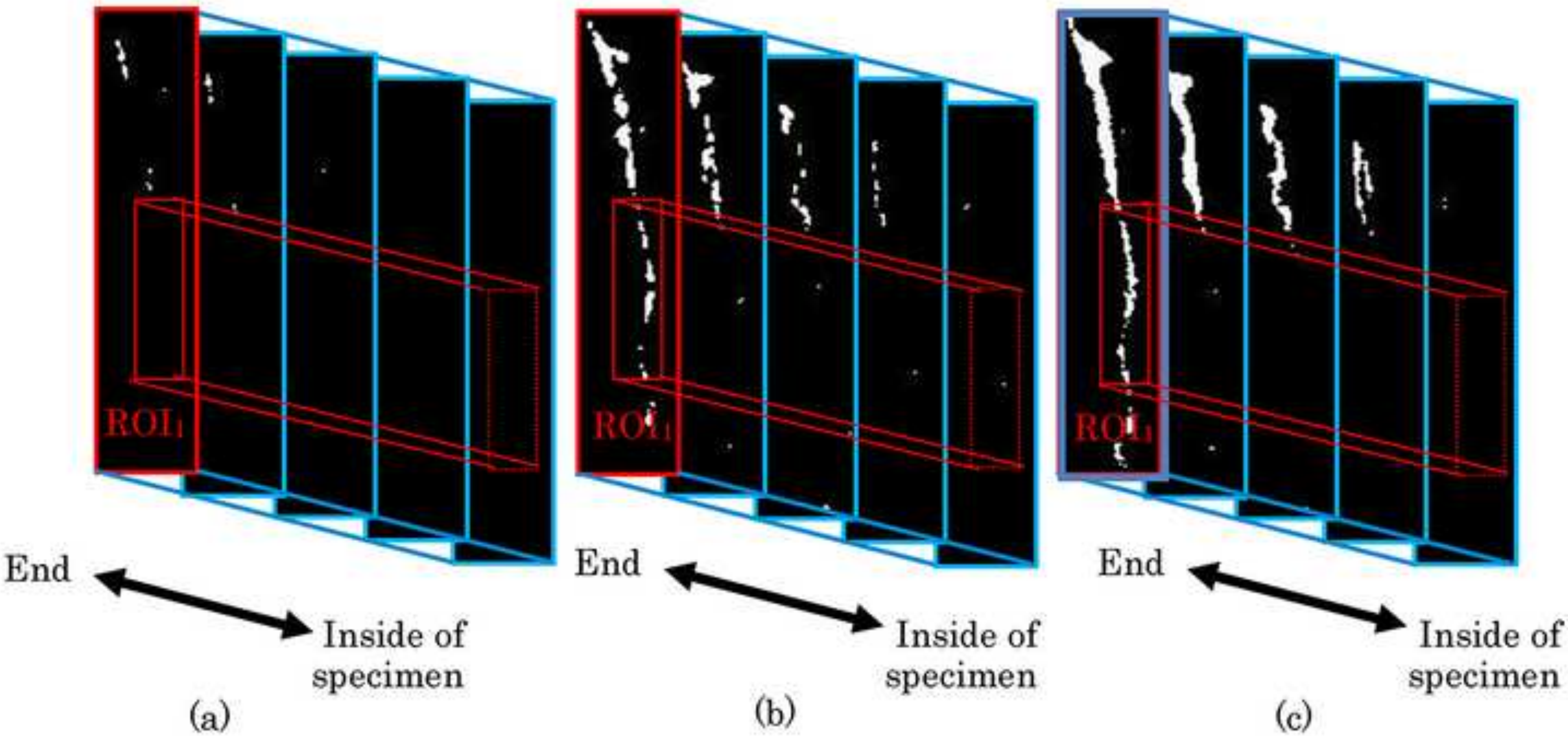

Figure10
Click here to download high resolution image

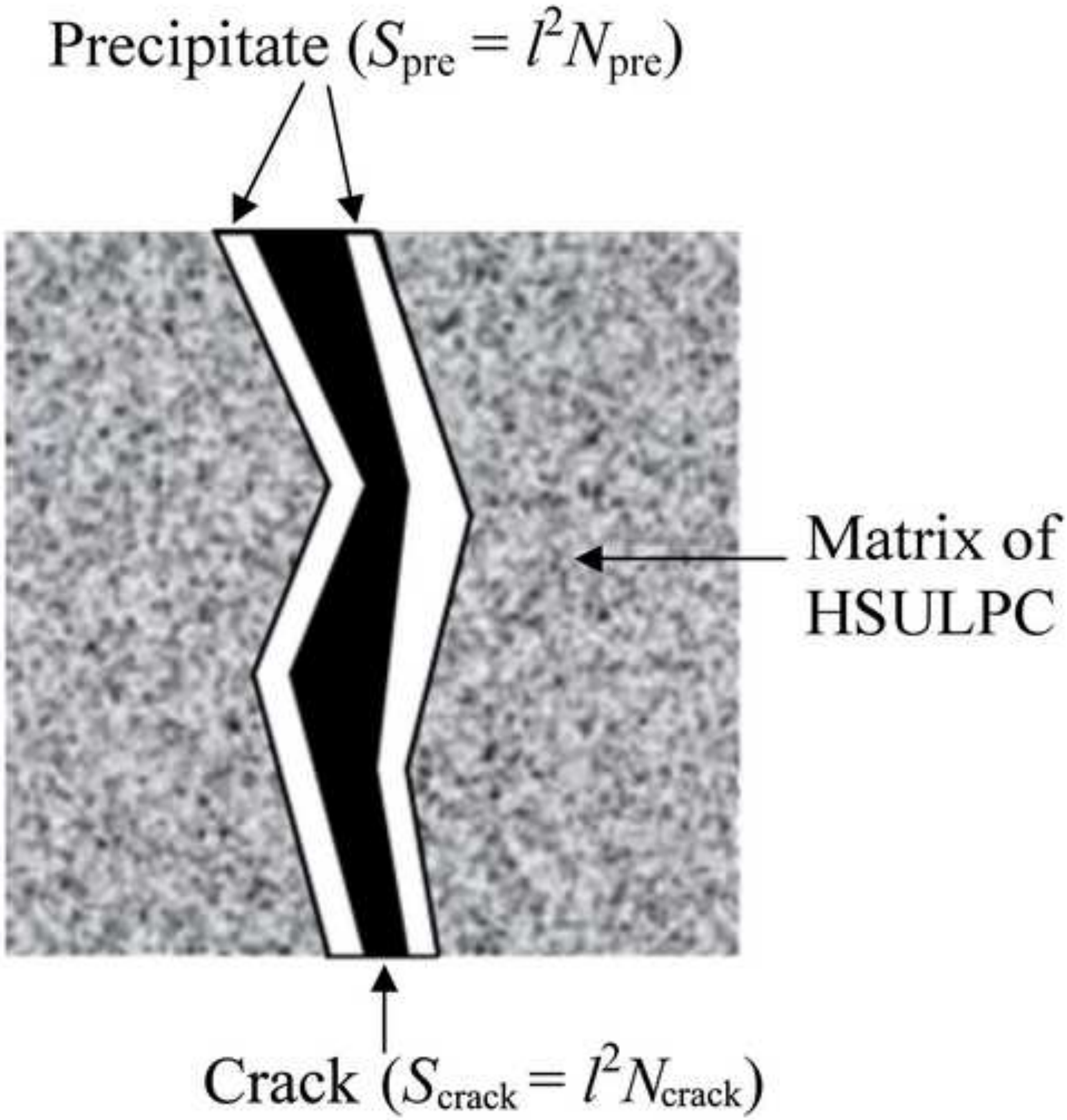

Figure11
Click here to download high resolution image

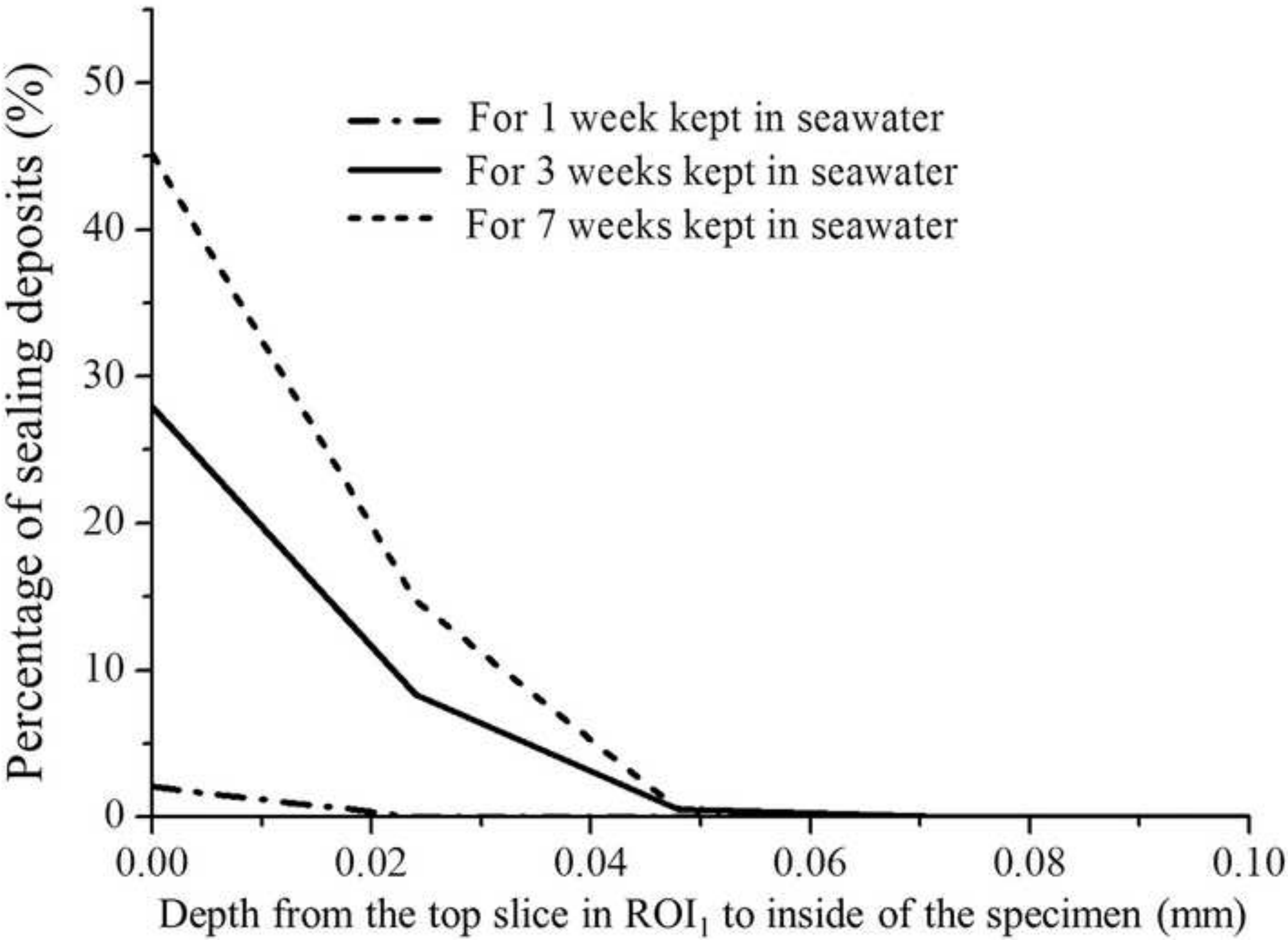

Figure12
Click here to download high resolution image